RM No. SL8A19

NACA

RESEARCH MEMORANDUM

for the

Bureau of Aeronautics, Department of the Navy

INVESTIGATION OF THE STABILITY AND CONTROL CHARACTERISTICS OF A $\frac{1}{10}$-SCALE MODEL OF THE CHANCE VOUGHT XF7U-1 AIRPLANE IN THE LANGLEY FREE-FLIGHT TUNNEL

TED No. NACA DE306

By

John W. Draper and Donald E. Hewes

Langley Memorial Aeronautical Laboratory
Langley Field, Va.

NATIONAL ADVISORY COMMITTEE FOR AERONAUTICS

WASHINGTON

NACA RM No. SL8A19 [redacted]

NATIONAL ADVISORY COMMITTEE FOR AERONAUTICS

RESEARCH MEMORANDUM

for the

Bureau of Aeronautics, Department of the Navy

INVESTIGATION OF THE STABILITY AND CONTROL CHARACTERISTICS OF A $\frac{1}{10}$-SCALE MODEL OF THE CHANCE VOUGHT XF7U-1 AIRPLANE IN THE LANGLEY FREE-FLIGHT TUNNEL

TED No. NACA DE306

By John W. Draper and Donald E. Hewes

SUMMARY

At the request of the Bureau of Aeronautics, Navy Department, a stability and control investigation of a $\frac{1}{10}$-scale model of the Chance Vought XF7U-1 airplane has been conducted in the Langley free-flight tunnel. Results of force and flight tests to determine the power-off stability and control characteristics of the model with slats retracted and extended are presented herein.

The longitudinal and lateral stability characteristics were satisfactory for both the slats retracted and extended conditions over the lift range up to the stall. With the slats retracted, the stall was fairly gentle but the model rolled off out of control. With the slats extended, control could be maintained at the stall so that the wings could be kept level even as the model dropped.

INTRODUCTION

An investigation of the low-speed power-off stability and control characteristics of a $\frac{1}{10}$-scale dynamic model of the Chance Vought XF7U-1 airplane has been conducted in the Langley free-flight wind tunnel at the request of the Bureau of Aeronautics, Navy Department. The XF7U-1 is a jet-propelled, sweptback, tailless fighter airplane, with twin vertical tails located midspan of the wings.

The present investigation consisted of power-off force and flight tests of the model with the slats retracted and extended. Tests to determine the effect of static margin on the longitudinal stability and control were included.

Comparison is made between the free-flight-tunnel low Reynolds number force-test results and higher Reynolds number force tests conducted at the Massachusetts Institute of Technology (M.I.T.) in order to permit a more accurate interpretation of the free-flight-test results in terms of the full-scale airplane.

SYMBOLS

All force and moment measurements are obtained with respect to the stability axes. A sketch showing the positive directions of the forces, moments, and angles is given in figure 1.

S	wing area, square feet
$\bar{c}$	mean geometric chord (M.G.C.), feet
b	wing span, feet
l	tail length (distance from center of gravity to centroid of area of vertical tails), feet
$\bar{z}$	height of center of pressure of vertical tails above fuselage horizontal center line, feet
V	airspeed, feet per second
q	dynamic pressure, pounds per square foot
ρ	air density, slugs per cubic foot
m	mass density, slugs per cubic foot
μ	relative density factor ($m/\rho Sb$)
k_X	radius of gyration about longitudinal body axis, feet
k_Y	radius of gyration about lateral body axis, feet
k_Z	radius of gyration about vertical body axis, feet
k_{XZ}	product of inertia factor about body axis, feet^2

γ flight-path angle, degrees

ϵ angle between reference axis and principal axis, positive when reference axis is above principal axis at the nose of the airplane, degrees

η angle of attack of principal axis of airplane, positive when principal axis is above flight-path axis (α - ϵ), degrees

α angle of attack of fuselage center line, degrees

β angle of sideslip, degrees

ψ angle of yaw, degrees

C_L lift coefficient (Lift/qS)

C_D drag coefficient (Drag/qS)

C_m pitching-moment coefficient (Pitching moment/qS$\bar{c}$)

C_Y lateral-force coefficient (Lateral force/qS)

C_n yawing-moment coefficient (Yawing moment/qSb)

C_l rolling-moment coefficient (Rolling moment/qSb)

δ_a ailavator deflection (perpendicular to hinge line), degrees

$C_{Y_{\delta_a}}$ rate of change of lateral-force coefficient per degree deflection of one ailavator $\left(\partial C_Y/\partial \delta_a\right)$

$C_{n_{\delta_a}}$ rate of change of yawing-moment coefficient per degree deflection of one ailavator $\left(\partial C_n/\partial \delta_a\right)$

$C_{l_{\delta_a}}$ rate of change of rolling-moment coefficient per degree deflection of one ailavator $\left(\partial C_l/\partial \delta_a\right)$

C_{Y_β} rate of change of lateral-force coefficient with angle of sideslip in degrees $\left(\partial C_Y/\partial \beta\right)$

C_{n_β} rate of change of yawing-moment coefficient with angle of sideslip in degrees $\left(\partial C_n/\partial \beta\right)$

C_{l_β} rate of change of rolling-moment coefficient with angle of sideslip in degrees $\left(\partial C_l/\partial \beta\right)$

Subscripts:

l left

r right

APPARATUS

The investigation was conducted in the Langley free-flight tunnel which is designed to test free-flying dynamic models. A description of the tunnel and test technique is presented in reference 1, and figure 2 shows the model flying in the test section. Force tests to determine the static aerodynamic characteristics of the model were made by using the free-flight-tunnel six-component balance which is described in reference 2.

A three-view drawing of the $\frac{1}{10}$-scale model used in the investigation is presented in figure 3 and photographs of the model are given in figure 4. Table I presents the dimensional and mass characteristics of the full-scale design in the landing condition and the scaled-up dimensional and mass characteristics of the model for both a light and a heavy condition.

The wing of the model had a modified Rhode St. Genese 35 airfoil section. The substitution of this section for the specified full-scale design section, CVA 4-(00)-(12)(40)-(1.1)(1.0), was in accordance with the free-flight-tunnel practice of using a high-lift airfoil which will obtain a maximum lift coefficient at low Reynolds numbers more nearly equal to that of the airplane than can be obtained by using the design airfoil. The ailavators were deflected upward to obtain the same basic pitching-moment characteristics as the design section, in preference to reflexing the full length of the trailing edge. The wing was set at 0° incidence with respect to the fuselage center line. The ailavator and flap plan forms were changed slightly from the full-scale design to simplify construction of the model. Intake-duct fairings were installed for most of the tests. (See figs. 3 and 4.)

The leading-edge slats used in the slats-extended force and flight tests were of a different design and plan form than those used on the full-scale airplane because a different airfoil section was used on the model. The details of the slat installation used on the model are shown in figure 5 and a photograph of the model with slats on is shown in figure 6.

TESTS

Tuft tests were made over the angle-of-attack range to determine the characteristics of the air flow over the wing with $\delta_a = -10^\circ$. These tests were made with and without the intake-duct fairings on.

Force tests were made to determine the aerodynamic similarity between the free-flight-tunnel $\frac{1}{10}$-scale model and the 0.145-scale model tested at M.I.T. at a Reynolds number of 2,500,000. Static longitudinal and lateral stability characteristics of the model were determined over an angle-of-attack range from zero through the stall for both the slat-retracted and slat-extended conditions. The static lateral-stability derivatives were determined for both the tail-off and tail-on configurations from the differences between lateral forces and moments measured at $\pm 5^\circ$ angles of yaw. The pitching effectiveness of the ailavators was determined for settings from -8° to -20° through the normal angle-of-attack range up to the stall. The rolling effectiveness of the ailavators was determined from tests with the left and right ailavators deflected to -35° and -5°, respectively.

All force tests were run at a dynamic pressure of 3.0 pounds per square foot, which corresponds to an air velocity of about 34 miles per hour at standard sea level and a Reynolds number of 420,000 based on the mean geometric chord (M.G.C.) of 1.31 feet. All forces and moments for the model are referred to a center-of-gravity position of 0.20 mean geometric chord and a vertical position of 0.0178 mean geometric chord above the fuselage horizontal center line, unless otherwise noted.

Flight tests were made to determine the dynamic stability and control characteristics of the model with slats retracted and extended. The flight tests covered a speed range from $C_L = 0.30$ to $C_L = 0.90$ for slats retracted and $C_L = 0.75$ to $C_L = 1.40$ with slats extended. In order to determine the effect of static margin $\left(\partial C_m/\partial C_L\right)$ on the longitudinal stability characteristics of the model, the center-of-gravity position was varied from 0.20 to 0.26 mean geometric chord with the trim ailavator setting lowered simultaneously to maintain a lift coefficient of about 0.75. This gave a range of static margin from -0.13 to 0.

Most of the flights were made with approximately correct moments of inertia but with the light wing loading (table I). This wing loading was used in order to minimize the damage to the model in crashes. A few tests were made at a lift coefficient of 0.5 with the heavy wing loading to determine whether the results of the more comprehensive tests at a light loading could be applied directly to the more heavily loaded condition. The heavy loading used for these tests corresponded approximately to the landing condition for the full-scale airplane.

CALCULATIONS

Boundaries for neutral lateral oscillatory stability (R = 0) were calculated for the model with the light wing loading condition and the slats retracted at lift coefficients of 0.4 and 0.8 by means of the stability equations of reference 3 and are shown in figure 7 as functions of C_{n_β} and $-C_{l_\beta}$.

The values of the static and dynamic lateral-stability derivatives were either obtained from force tests or estimated from unpublished data and are presented in table II.

RESULTS AND DISCUSSION

Tuft Tests

The results of the tuft surveys made to determine the air-flow characteristics over the wing are shown in figure 8. These results indicate that the blunt, sealed air-intake ducts (fig. 3) induced a premature stall at the wing roots. Fairing the intake-duct opening produced satisfactory flow conditions which probably simulate fairly well the air flow over the full-scale airplane with ducts open. Therefore, all force-test data presented in this paper were obtained with fairings on. (See figs. 3 and 4.)

Force Tests

The results of force tests made to determine the static longitudinal and lateral stability characteristics of the model are presented in figures 9 to 14. These figures also include data from tests conducted at M.I.T.

Longitudinal stability.- The results presented in figure 8 show the effect of the slats on the longitudinal stability characteristics of the free-flight-tunnel model. It is seen that with slats retracted, the stability of the model increased with increase in lift coefficient and the model was stable at the stall. Extending the slats decreased the stability over the lift range and resulted in an indication of slight static instability at the stall. The slats increased the maximum lift coefficient from 0.88 to 1.38.

A comparison of the longitudinal data for the free-flight-tunnel model and data from M.I.T. is shown in figure 10 for the slat-retracted

and slat-extended conditions. It should be noted that the free-flight-tunnel slat-extended data have been transferred to 0.17 mean geometric chord center-of-gravity location because the M.I.T. slat-extended data were obtained at this center-of-gravity location and drag data were not available for transfer purposes. The maximum lift coefficients for both conditions are in fairly good agreement and the longitudinal stability $\left(\partial C_m/\partial C_L\right)$ is about the same at lower lift coefficients. At the higher lift coefficients with slats retracted the free-flight-tunnel model had slightly greater stability than the M.I.T. model while the M.I.T. model had greater stability with slats extended. Both models showed slight instability at the stall with slats extended.

The pitching effectiveness of the ailavators with slats retracted, shown in figure 11, was reduced as C_L increased. This figure also shows that the static margin increased with C_L and $-\delta_a$.

Lateral stability.- The lateral-stability parameters $-C_{l_\beta}$, C_{n_β}, and C_{Y_β}, for the free-flight-tunnel model are compared with those for the M.I.T. model in figure 12. The directional stability and effective dihedral parameters, C_{n_β} and $-C_{l_\beta}$, of both models with slats retracted increased with lift coefficient and are in fairly good agreement below $C_L = 0.7$. Above this value, the parameters of the free-flight-tunnel model drop below those of the M.I.T. model. It can be seen by comparing the tails-on and tails-off curves for the free-flight-tunnel model that this drop is caused by the characteristics of the wing and not by any decrease in vertical-tail effectiveness. There are no M.I.T. data available for a comparison of the slat-extended condition.

The results of the tests made to determine the rolling effectiveness of the ailavators are presented in figure 13. With slats retracted the rolling moment for the free-flight model was nearly constant up to the stall where there was a small decrease in effectiveness. Extending the slats had little effect on the rolling moment, and the agreement of the free-flight-tunnel and M.I.T. data was fairly good over the range covered. The ailavators produced favorable yaw up to the stall with the slats retracted, and the agreement of the free-flight-tunnel and M.I.T. data was very good. Extending the slats had little effect on the ailavator yawing moment except in the range of the extended lift coefficient where the yawing moment became adverse at a lift coefficient of about $C_L = 0.95$ and remained adverse through the stall. The favorable yawing moment was previously noted in tests of an 0.08-scale model of the XF7U-1 in the Langley high-speed 7- by 10-foot tunnel (reference 4) and was attributed to the side force on the vertical tails induced by the deflected ailavators. The increased load on the outboard portion of the wing ahead of the down-going aileron produces a more outward air

flow which strikes the vertical tail and results in a favorable yawing moment. Conversely, the tip load on the other wing is decreased by the aileron being deflected up, and this causes less outward flow along the wing which produces an additional favorable yawing moment.

Since the aerodynamic characteristics of the free-flight-tunnel model were in fairly good agreement with those from the higher-scale M.I.T. tests, the flight characteristics of the free-flight model should be fairly representative of those of the full-scale airplane.

Flight Tests

Longitudinal stability.- The longitudinal stability of the model with slats extended and retracted was satisfactory throughout the speed ranges covered in the flight tests $\left(C_L = 0.30\right.$ to the stall for slats retracted and $C_L = 0.75$ to the stall for slats extended$\left.\right)$. It was necessary to increase the ailavator deflections to maintain effective longitudinal control near the stall. This was evidently because of greater static longitudinal stability at high lift coefficients and the loss of ailavator effectiveness at large deflections which was shown by force tests (fig. 11). The model was longitudinally stable at the stall with the slats both extended and retracted although force tests indicated slight static instability at the stall with the slats extended.

The results of the flight tests made to determine the effect of $\partial C_m/\partial C_L$ on the longitudinal flight characteristics are summarized in the following table. Force-test data for some of these flight-test conditions are presented in figure 14.

(Slats retracted; $C_L = 0.75$)

Center-of-gravity position, percent mean geometric chord	δ_a (deg)	$\partial C_m/\partial C_L$	Comments
21.7	-22	-0.13	Very stable longitudinally. Easy to control.
23.0	-18	-.10	Do.
24.3	-15	-.08	Do.
25.0	-13.5	-.06	Noticeable sensitivity to longitudinal disturbances.
25.2	-12	-.04	Increased sensitivity. More attention to elevator control required
25.7	-10	-.02	Difficult to hold steady in center of tunnel. Required constant elevator control.
26.2	-8	0	Uncontrollable. Impossible to fly because of divergent pitching oscillations.

The longitudinal flight characteristics were considered to be satisfactory with $\partial C_m/\partial C_L$ as low as -0.06. For flights below this value, increasing sensitivity to longitudinal disturbances that required more attention to elevator control was noted. The amplitude of the model's motion due to a disturbance increased as $\partial C_m/\partial C_L$ was reduced. With zero $\partial C_m/\partial C_L$, the model became uncontrollable and divergent pitching oscillations resulted in the model crashing to the tunnel floor.

Lateral stability.- Directional stability and effective dihedral for both slats retracted and extended were adequate over the flight range. All oscillations observed were small and well damped. The results of the calculations (fig. 7) show that the model flight-test points as represented by C_{n_β} and $-C_{l_\beta}$ at $C_L = 0.4$ and $C_L = 0.8$ were within the stable region of their respective boundaries. The calculations indicate a reduction in oscillatory stability as the lift coefficient is decreased. Lateral control was as good with ailerons alone as with coordinated aileron and rudder. At the stall, with slats retracted, lateral control became weaker and the model rolled and slipped off and could not be prevented from crashing into the tunnel wall. If more space had been

available in the tunnel test section, however, recovery from the stall might have been possible. With the slats extended, lateral control was maintained at the stall so that the wings could be kept level even while the model dropped to the floor of the tunnel.

There was no apparent change in flight characteristics when the wing loading was increased from the light to the heavy condition.

CONCLUSIONS

The following conclusions were drawn from the results of the free-flight-tunnel power-off stability and control investigation. Since the aerodynamic characteristics of the free-flight-tunnel model were in fairly good agreement with those from the M.I.T. tests made at a higher Reynolds number, the flight characteristics of the free-flight model are believed to be generally representative of those of the full-scale airplane.

1. The model was longitudinally stable through flight ranges of $C_L = 0.30$ to the stall with slats retracted and $C_L = 0.75$ to the stall with slats extended.

2. With the slats retracted, the stall was gentle but the model rolled and slid off into the tunnel wall out of control. With the slats extended, control could be maintained at the stall so that the wings could be kept level even as the model dropped.

3. Lateral stability was considered satisfactory for all conditions with slats extended or retracted. All oscillations were small and well damped and there was no noticeable adverse yaw due to ailerons.

Langley Memorial Aeronautical Laboratory
National Advisory Committee for Aeronautics
Langley Field, Va.,

John W. Draper
Aeronautical Engineer

Donald E. Hewes
Aeronautical Engineer

Approved: Thomas A. Harris
Thomas A. Harris
Chief of Stability Research Division

bwb

REFERENCES

1. Shortal, Joseph A., and Osterhout, Clayton J.: Preliminary Stability and Control Tests in the NACA Free-Flight Wind Tunnel and Correlation with Full-Scale Flight Tests. NACA TN No. 810, 1941.

2. Shortal, Joseph A., and Draper, John W.: Free-Flight-Tunnel Investigation of the Effect of the Fuselage Length and the Aspect Ratio and Size of the Vertical Tail on Lateral Stability and Control. NACA ARR No. 3D17, 1943.

3. Sternfield, Leonard: Effect of Product of Inertia on Lateral Stability. NACA TN No. 1193, 1947.

4. Goodson, Kenneth W., and Myers, Boyd C., II: An Investigation of the Aerodynamic Characteristics of an 0.08-Scale Model of the Chance Vought XF7U-1 Airplane in the Langley High-Speed 7- by 10-Foot Tunnel. Part IV - Aileron Characteristics. - TED No. NACA DE306. NACA RM No. L7H22, Bur. Aero., 1947.

CONFIDENTIAL

TABLE I

DIMENSIONAL AND MASS CHARACTERISTICS OF CHANCE VOUGHT XF7U-1

AND SCALED-UP CHARACTERISTICS OF $\frac{1}{10}$-SCALE MODEL TESTED

IN LANGLEY FREE-FLIGHT TUNNEL

	Scaled-up Light	Scaled-up Heavy	Full-scale (landing condition)
Weight, lb	7,710	12,600	12,400
Wing loading, W/S, lb/sq ft	15.5	25.4	25.0
Relative density factor, μ, $(m/\rho Sb)$	5.23	8.55	8.41
Center-of-gravity location, percent M.G.C.	20	20	20
Moments of inertia:			
I_X, slug-ft^2	12,520	15,320	11,820
I_Y, slug-ft^2	17,770	24,480	21,650
I_Z, slug-ft^2	29,200	37,220	32,350
Radius of gyration to wing span:			
k_X/b	0.187	0.163	0.145
k_Y/b	0.223	0.205	0.193
k_Z/b	0.285	0.254	0.236
Wing:			
Airfoil section:			
Scaled-up	Modified RSG-35		
Full-scale			CVA 4-(00)(12)(40) - (1.1)(1.0)
Area, sq ft	496		496
Span, ft	38.8		38.8
Aspect ratio	3.0		3.0
Sweepback, c/4, deg	35		35
Incidence, deg	0		0
Dihedral, deg	0		0
Taper ratio	0.6		0.6
Washout, deg	0		0
M.G.C., ft	13.1		13.1
Location of leading-edge M.G.C. behind leading edge root chord, ft	6.96		6.96
Root chord, ft	16.0		16.0
Tip chord, ft	9.67		9.67
Distance from nose to leading-edge root chord, ft	9.46		9.46
Ailavators:			
Area, percent wing area, (one)	9.7		11
Span, percent semi-wing span, (one)	43		47.7
Chord, percent wing chord (inboard)	22.9		22.5
Chord, percent wing chord (outboard)	29.2		29.0
Slat:			
Type	Constant percentage chord		Constant chord
Location, percent semispan:			
Inboard	16.6		16.6
Outboard	96.0		96.0
Vertical tail:			
Area, sq ft (total)	244.8		244.8
Vertical tail length (distance along X-axis from 20-percent M.G.C. station to centroid of area of vertical tail), ft	11.0		11.0

CONFIDENTIAL

[redacted]

TABLE II

CHARACTERISTICS OF MODEL USED IN CALCULATIONS OF NEUTRAL LATERAL OSCILLATORY STABILITY BOUNDARIES (R = 0)

	$C_L = 0.8$	$C_L = 0.4$
W	7.71	7.71
W/S	1.56	1.56
b	3.87	3.87
ρ	.00238	.00238
V	40.4	57.1
μ	5.23	5.23
k_X	.724	.724
k_Z	1.105	1.105
k_{X_Z}	-.016	-.016
l/b	.284	.284
$\bar{z}/b$	.058	.058
γ	-7.0	-8.0
α	15.5	8.0
ϵ	-1.0	-1.0
η	16.5	9.0
$^1C_{y_\beta}$	$-0.100 + C_{y_{\beta(tail)}}$	$-0.0745 + C_{y_{\beta(tail)}}$
$^1C_{n_\beta}$	$0.020 + C_{n_{\beta(tail)}}$	$0.0115 + C_{n_{\beta(tail)}}$
$^1C_{l_p}$	$-0.25 + C_{l_{p(tail)}}$	$-0.25 + C_{l_{p(tail)}}$
$^1C_{n_p}$	$-0.004 + C_{n_{p(tail)}}$	$-0.075 + C_{n_{p(tail)}}$
$^1C_{l_r}$	$0.12 + C_{l_{r(tail)}}$	$0.092 + C_{l_{r(tail)}}$
$^1C_{n_r}$	$-0.020 + C_{n_{r(tail)}}$	$-0.0117 + C_{n_{r(tail)}}$
$C_{y_{\beta(tail)}}$	^{2}Variable	^{2}Variable

^{1}Tail contributions are determined from the following equations:

$$C_{n_{\beta(tail)}} = -\frac{l}{b} C_{y_{\beta(tail)}}$$

$$C_{l_{p(tail)}} = 2\left(\frac{\bar{z}}{b} - \frac{l}{b}\sin\alpha\right)^2 C_{Y_{\beta(tail)}}$$

$$C_{n_{p(tail)}} = C_{l_{r(tail)}} = -2\frac{l}{b}\left(\frac{\bar{z}}{b} - \frac{l}{b}\sin\alpha\right) C_{Y_{\beta(tail)}}$$

$$C_{n_{r(tail)}} = 2\left(\frac{l}{b}\right)^2 C_{Y_{\beta(tail)}}$$

^{2}Varied systematically as independent variable to provide the desired range of C_{n_β} for the determination of the stability boundaries.

[redacted]

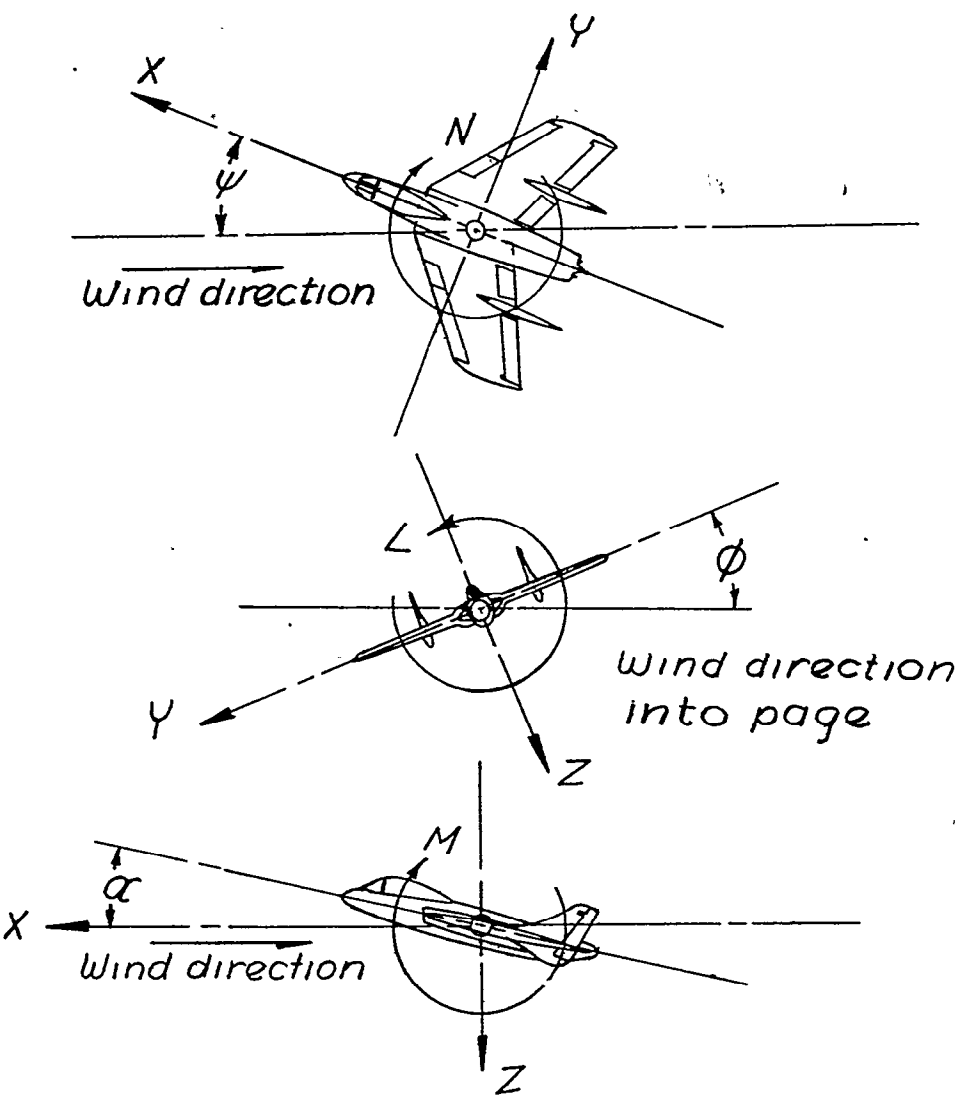

Figure 1.- The stability system of axes. Arrows indicate positive directions of moments and forces. This system of axes is defined as an orthagonal system having its origin at the center of gravity and in which the Z-axis is in the plane of symmetry and perpendicular to the relative wind, the X-axis is in the plane of symmetry and perpendicular to the Z-axis, and the Y-axis is perpendicular to the plane of symmetry.

NATIONAL ADVISORY
COMMITTEE FOR AERONAUTICS

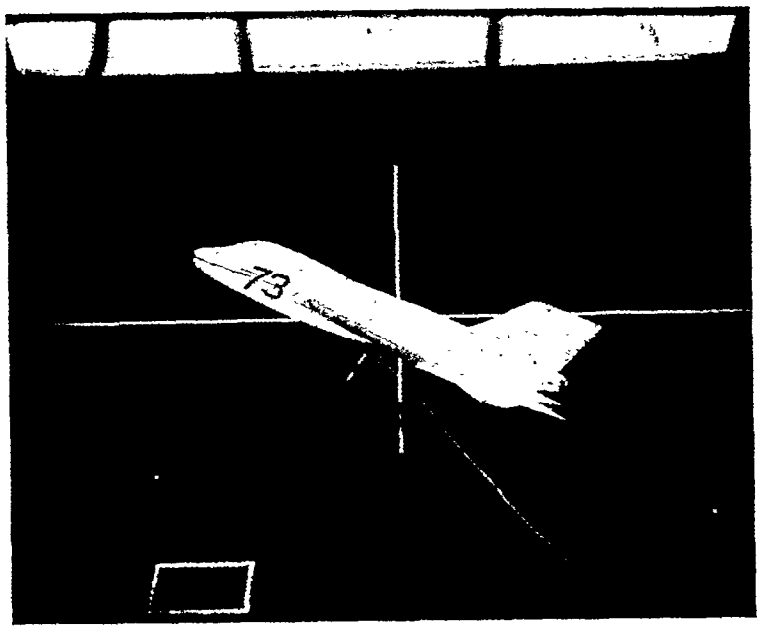

(a) Side view.

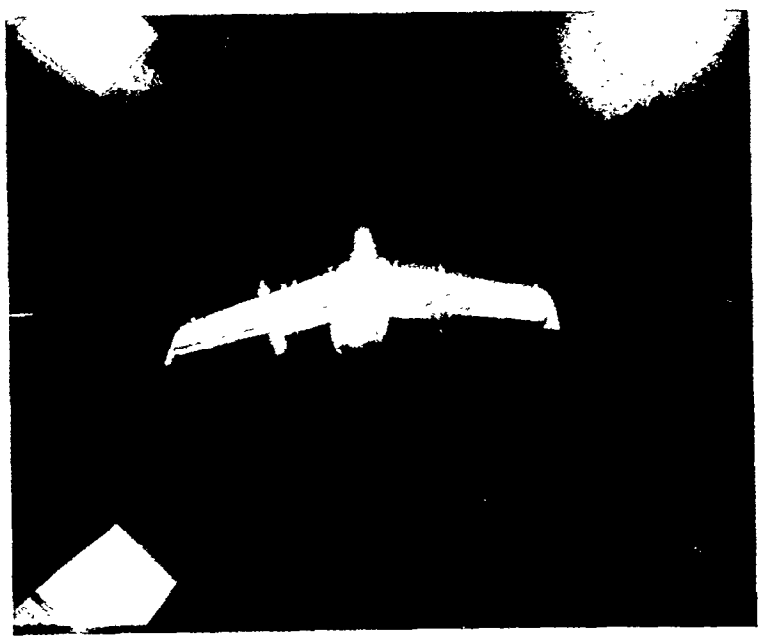

(b) Rear view.

Figure 2.- Photographs of $\frac{1}{10}$-scale model of Chance Vought XF7U-1 airplane flying in the Langley free-flight tunnel. Leading-edge slat extended.

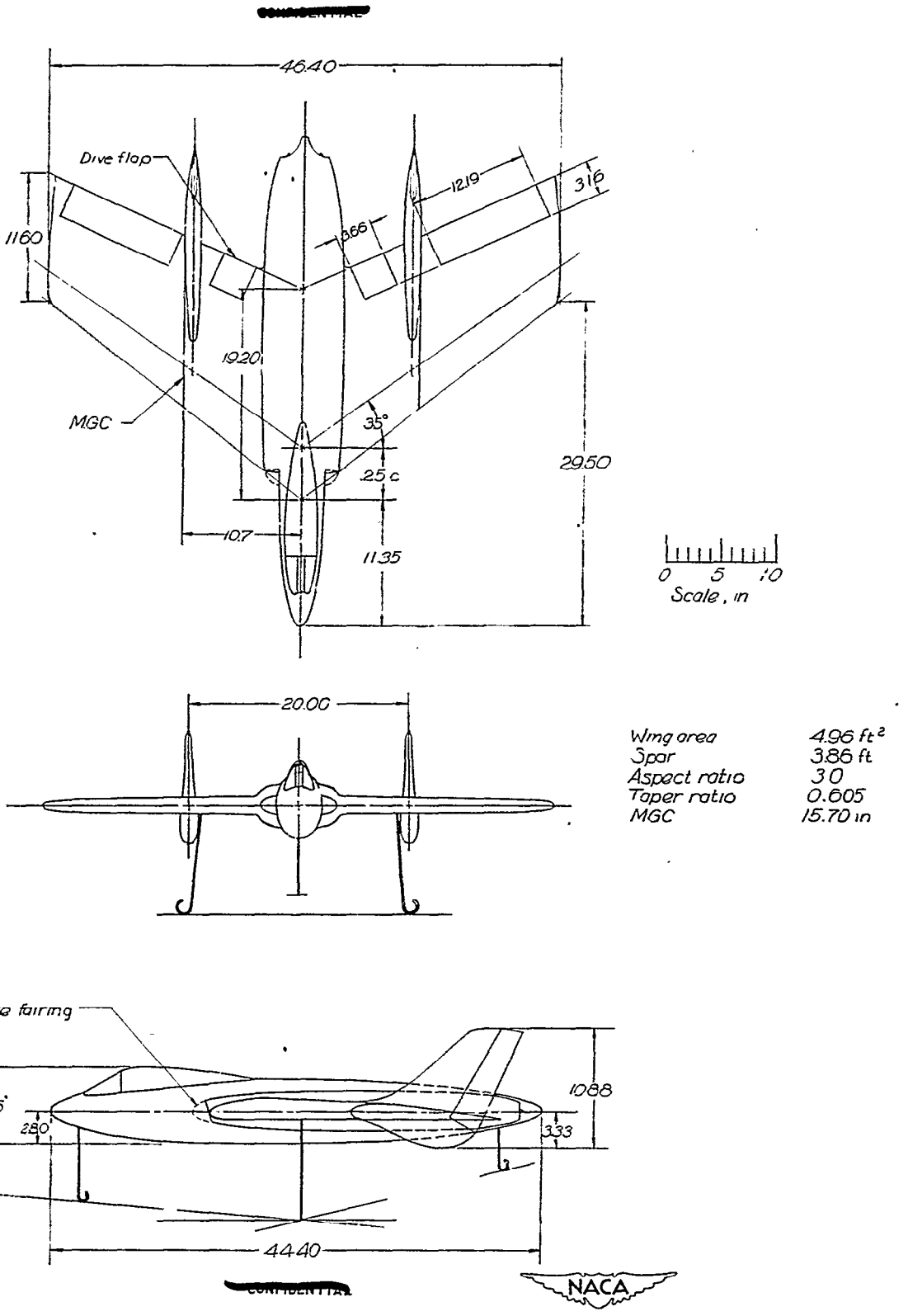

Figure 3.- Three-view drawing of the 1/10-scale model of the Chance Vought XF7U-1 tested in the Langley free-flight tunnel.

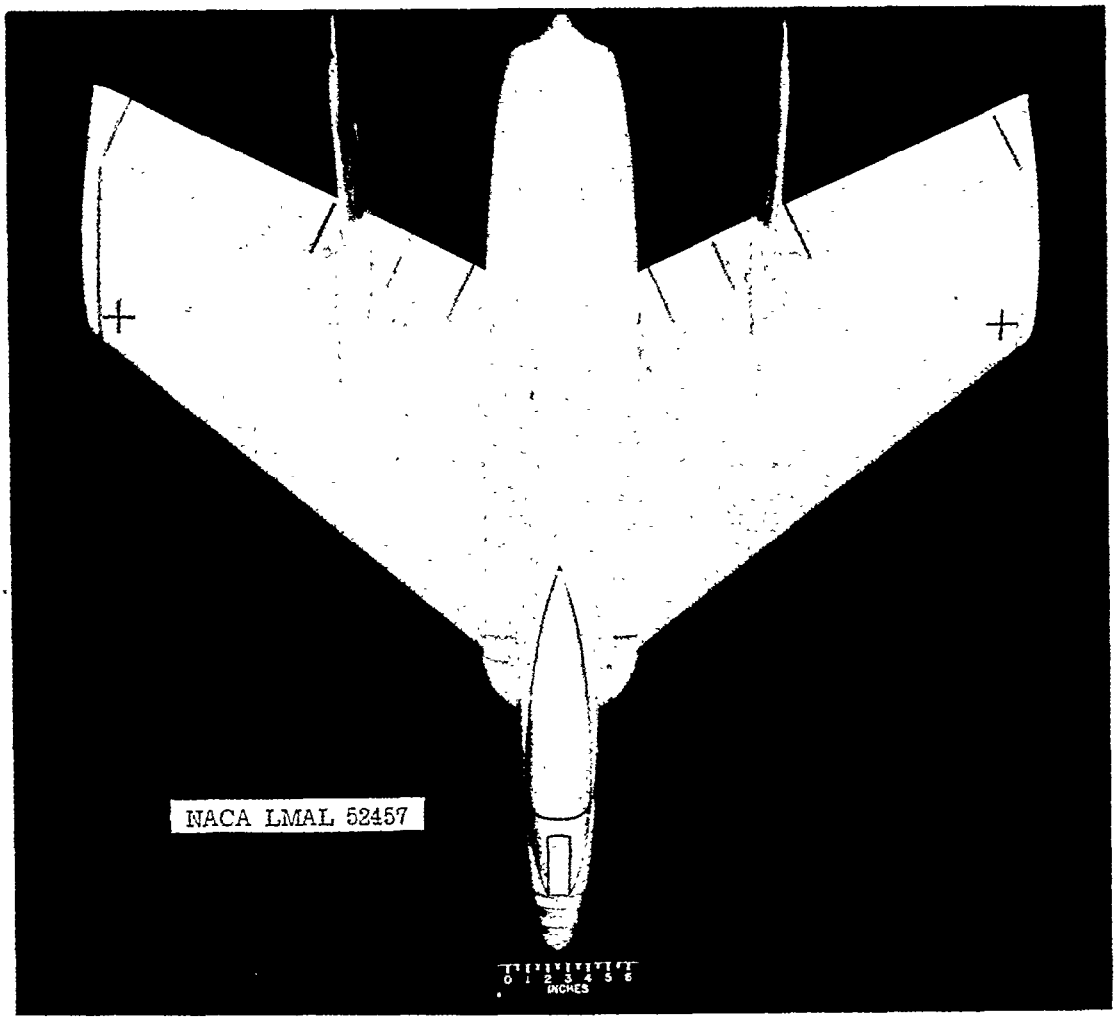

(a) Top view.

Figure 4.- Langley free-flight-tunnel $\frac{1}{10}$-scale model of Chance Vought XF7U-1 with slats retracted.

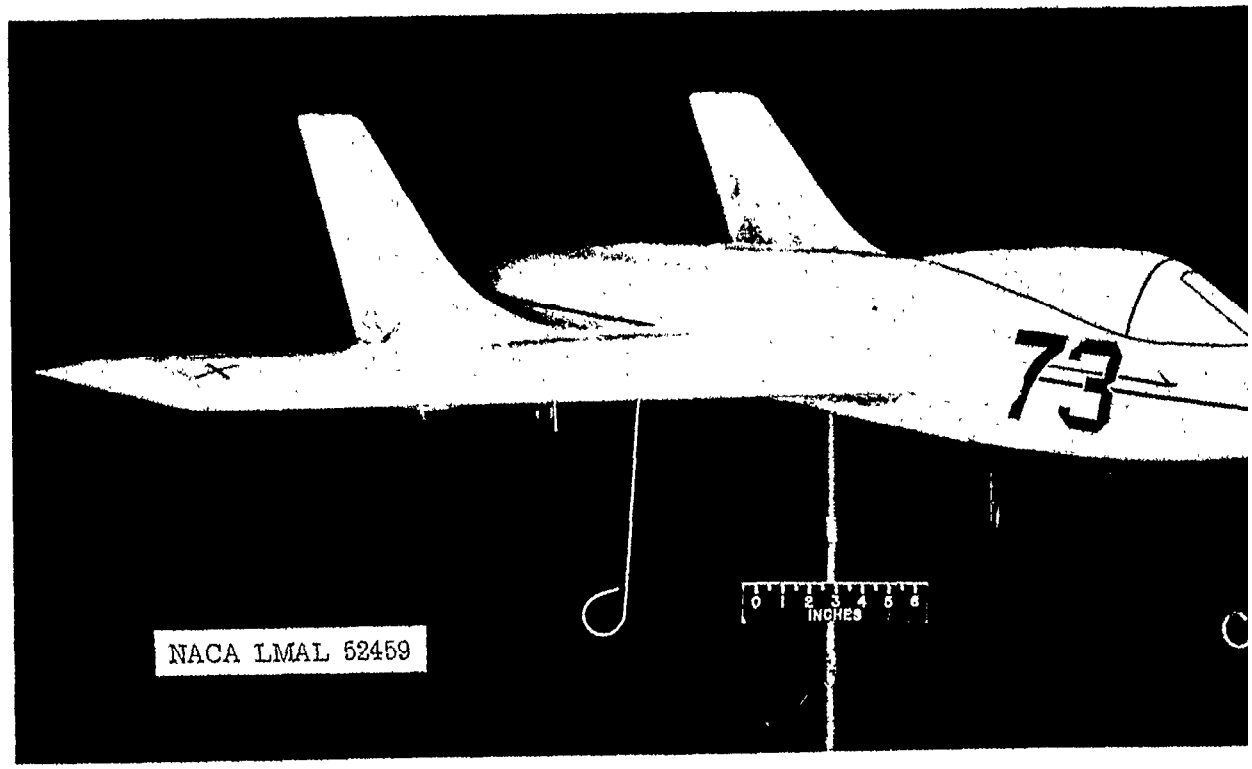

(b) Three-quarter front view.

Figure 4.- Continued.

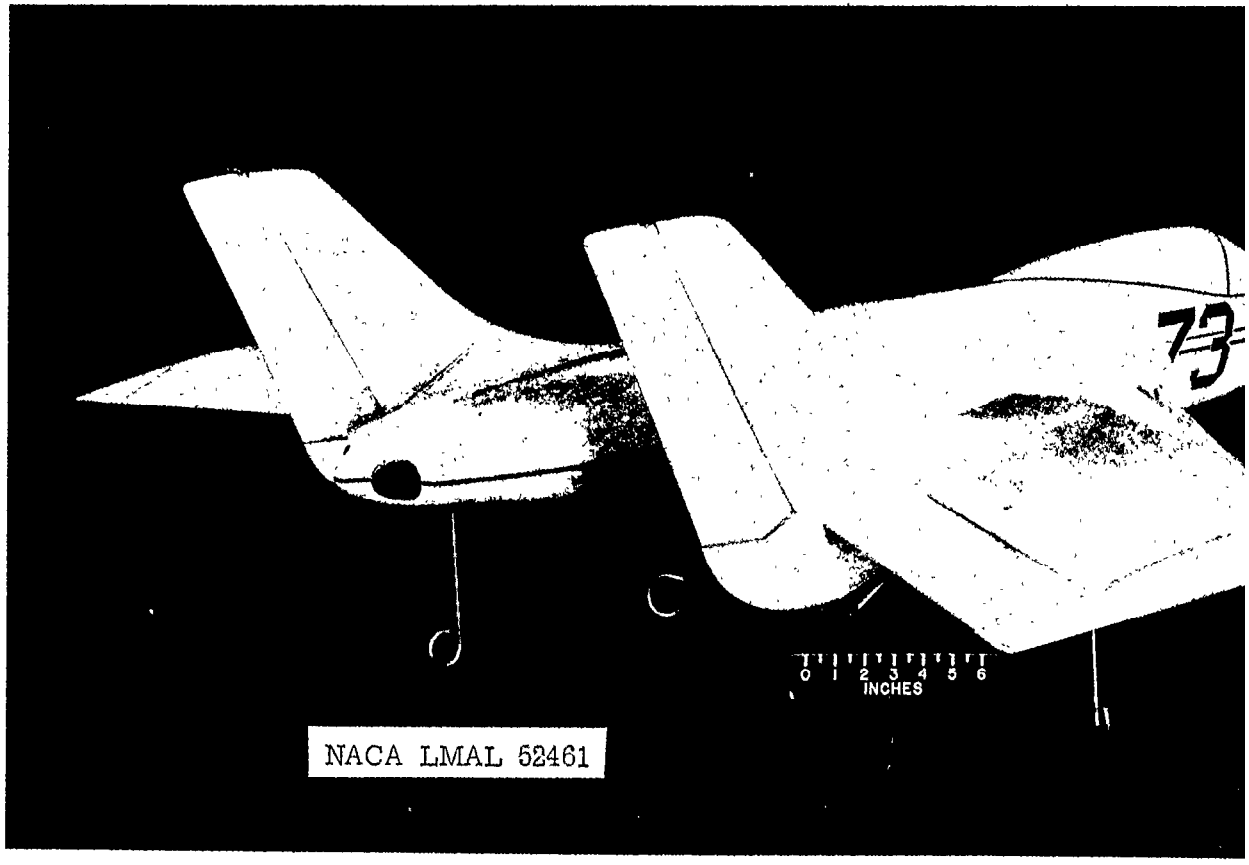

(c) Three-quarter rear view.

Figure 4.- Concluded.

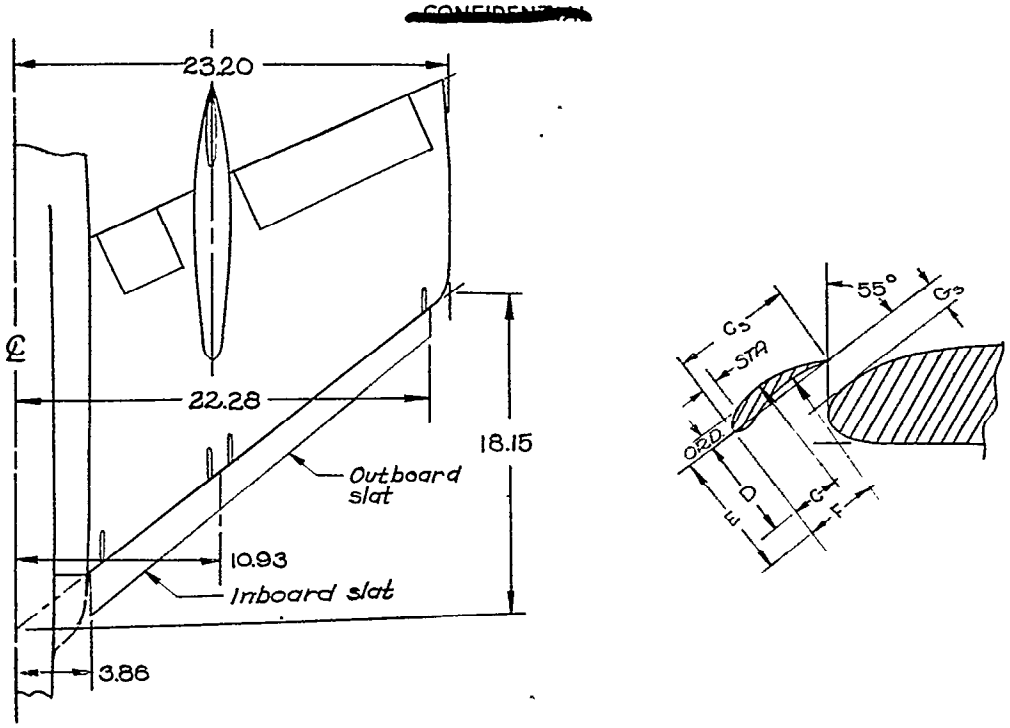

Ordinates of slat airfoil section (parallel to ℄)

Station 3.86			Station 10.93			Station 22.28		
Station	Lower	Upper	Station	Lower	Upper	Station	Lower	Upper
0	-.057	.115	0	-.050	.100	0	-.038	.088
.050	.022	.174	.044	.019	.152	.036	.014	.116
.103	.033	.230	.090	.029	.201	.073	.022	.154
.156	.041	.275	.136	.036	.240	.109	.027	.183
.208	.036	.316	.182	.031	.276	.145	.024	.210
.259	.031	.347	.226	.027	.303	.182	.020	.230
.391	.007	.400	.341	.006	.349	.272	.005	.267
.520	-.031	.435	.454	-.027	.380	.365	-.020	.290
.778	-.101	.474	.679	-.088	.414	.546	-.067	.316
C	.914		C	.798		C	.559	
D	2.830		D	2.471		D	1.884	
E	3.375		E	2.947		E	2.262	
F	1.482		F	1.294		F	.986	
C_S	2.600		C_S	2.27		C_S	1.73	
G_S	.716		G_S	.625		G_S	.480	

(Note: C_S and G_S are 14.5 and 4 percent, respectively, of wing chord)

Figure 5.- Details of slat installation used on $\frac{1}{10}$-scale model of Chance Vought XF7U-L

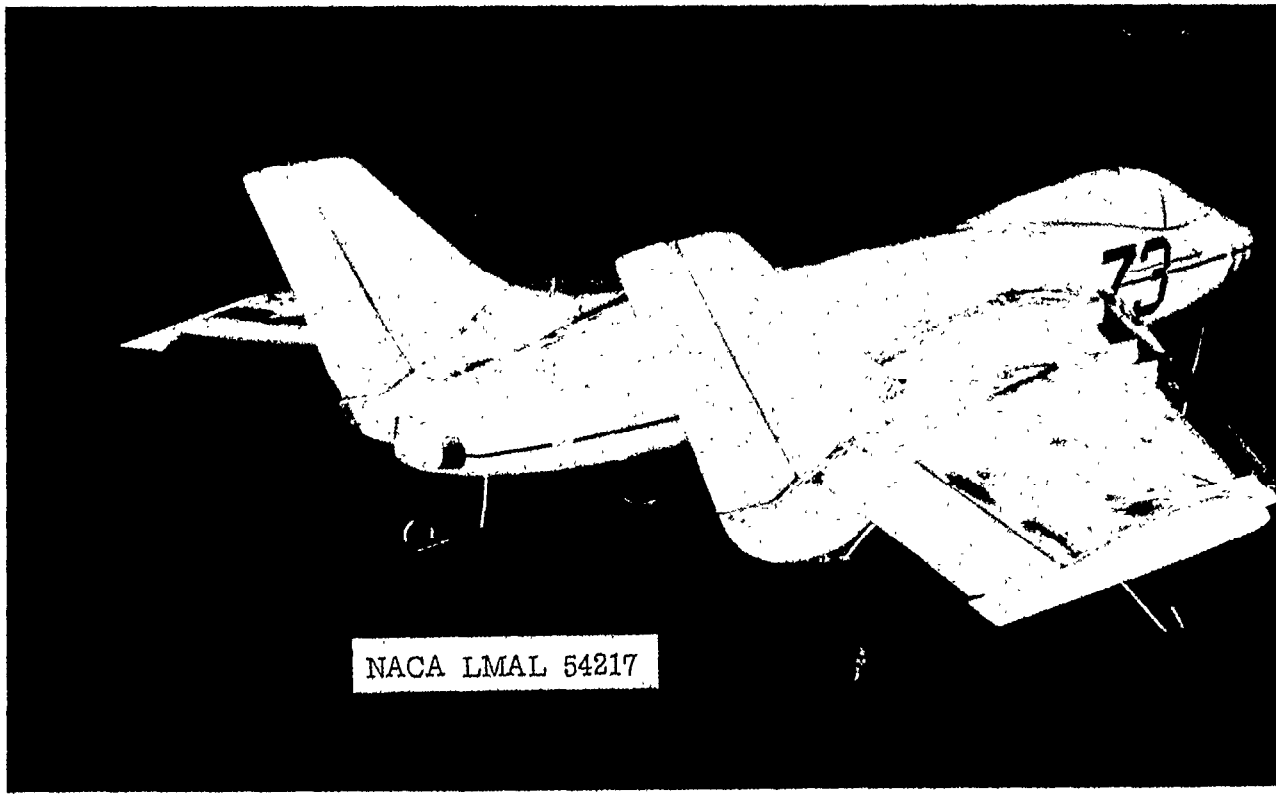

Figure 6.- Three-quarter rear view of $\frac{1}{10}$-scale model of Chance Vought XF7U-1 v

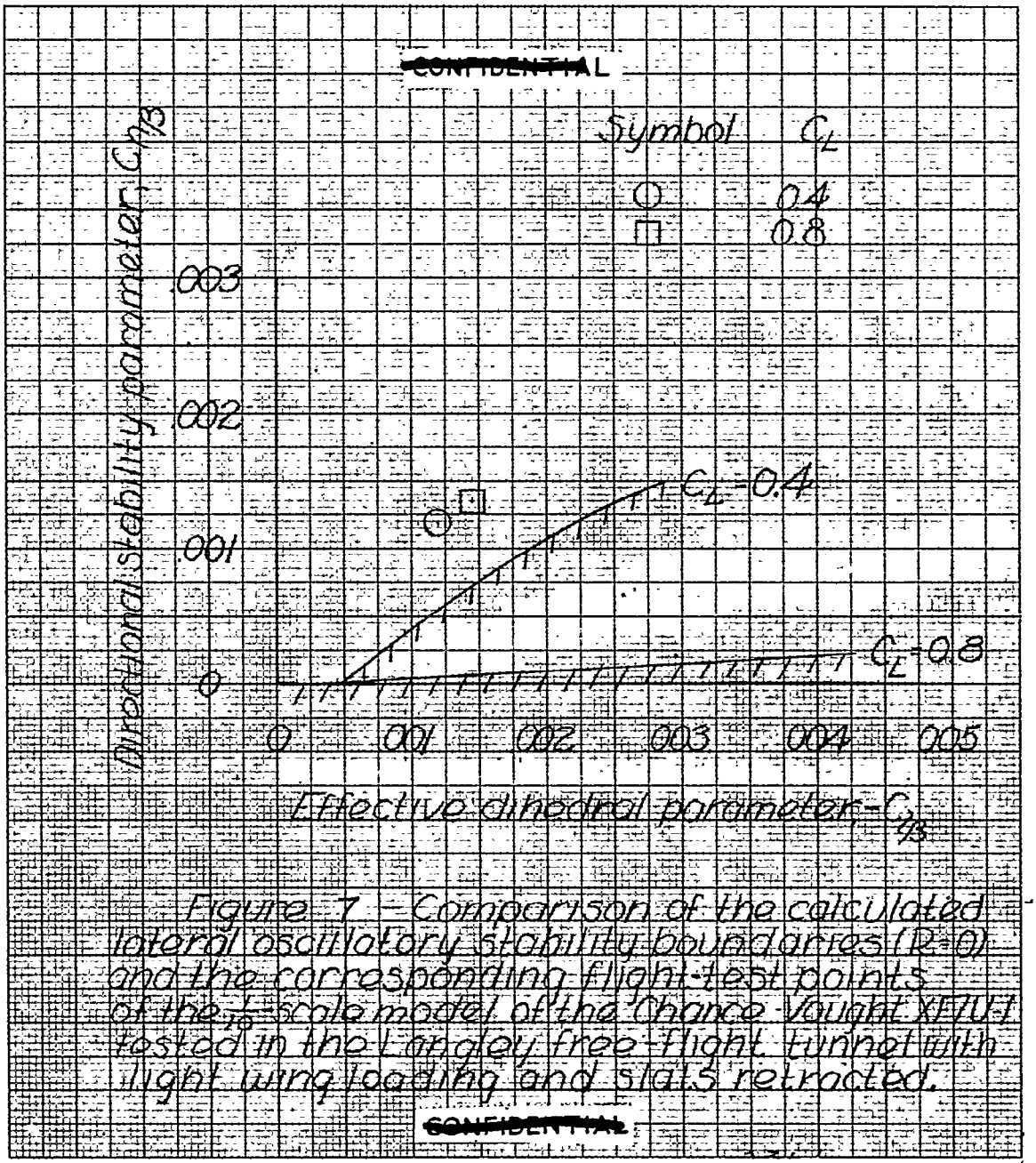

Figure 7 - Comparison of the calculated lateral oscillatory stability boundaries ($k_2 = 0$) and the corresponding flight-test points of the 1/10-scale model of the Chance Vought XF7U-1 tested in the Langley free-flight tunnel with flight wing loading and slats retracted.

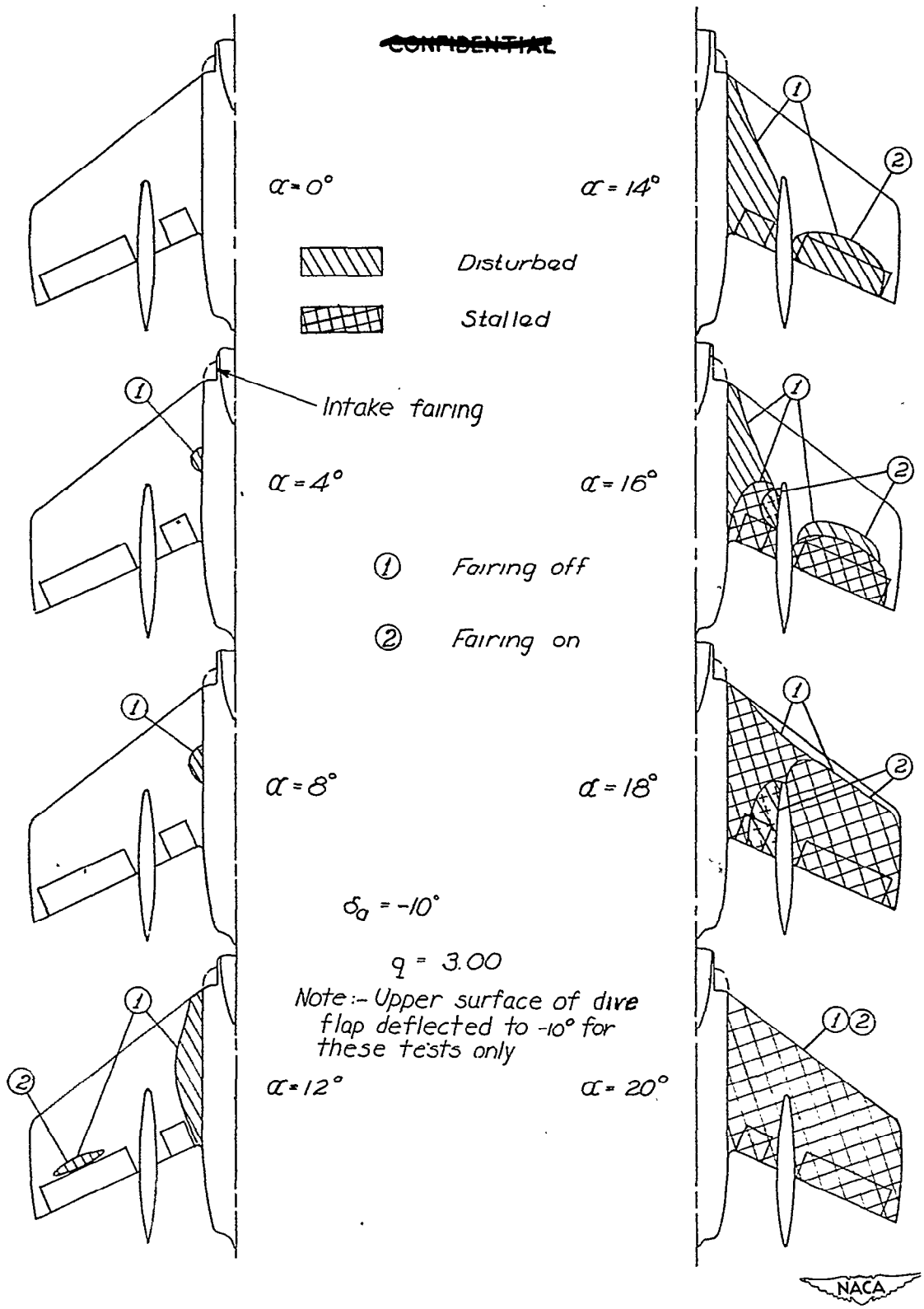

Figure 8.- Tuft survey of Langley FFT 1/6-scale model of Chance Vought XF7U-1 with slats retracted.

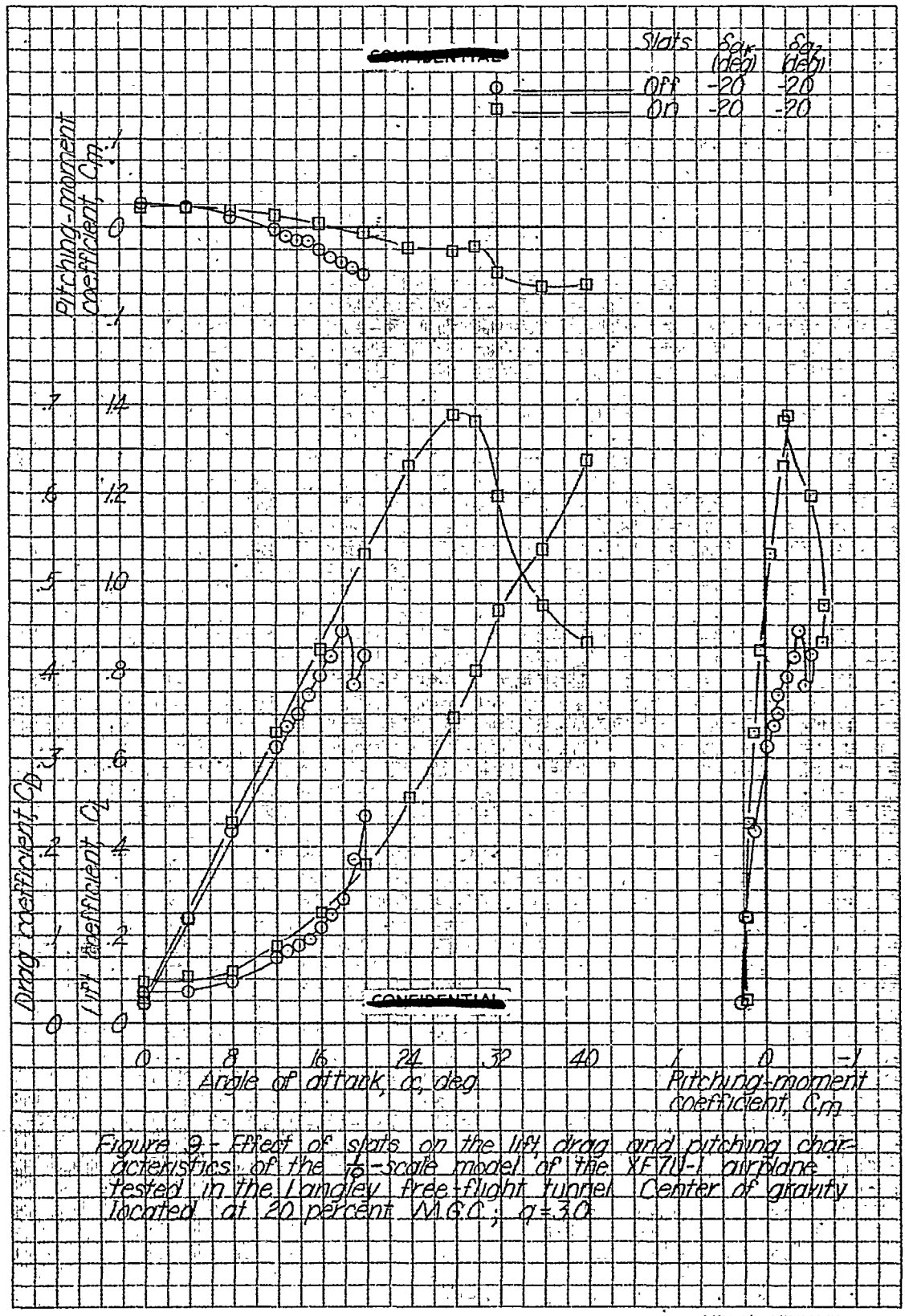

Figure 9.- Effect of slats on the lift, drag, and pitching characteristics of the 1/10-scale model of the XF7U-1 airplane tested in the Langley free-flight tunnel. Center of gravity located at 20 percent M.G.C.; $q = 30$.

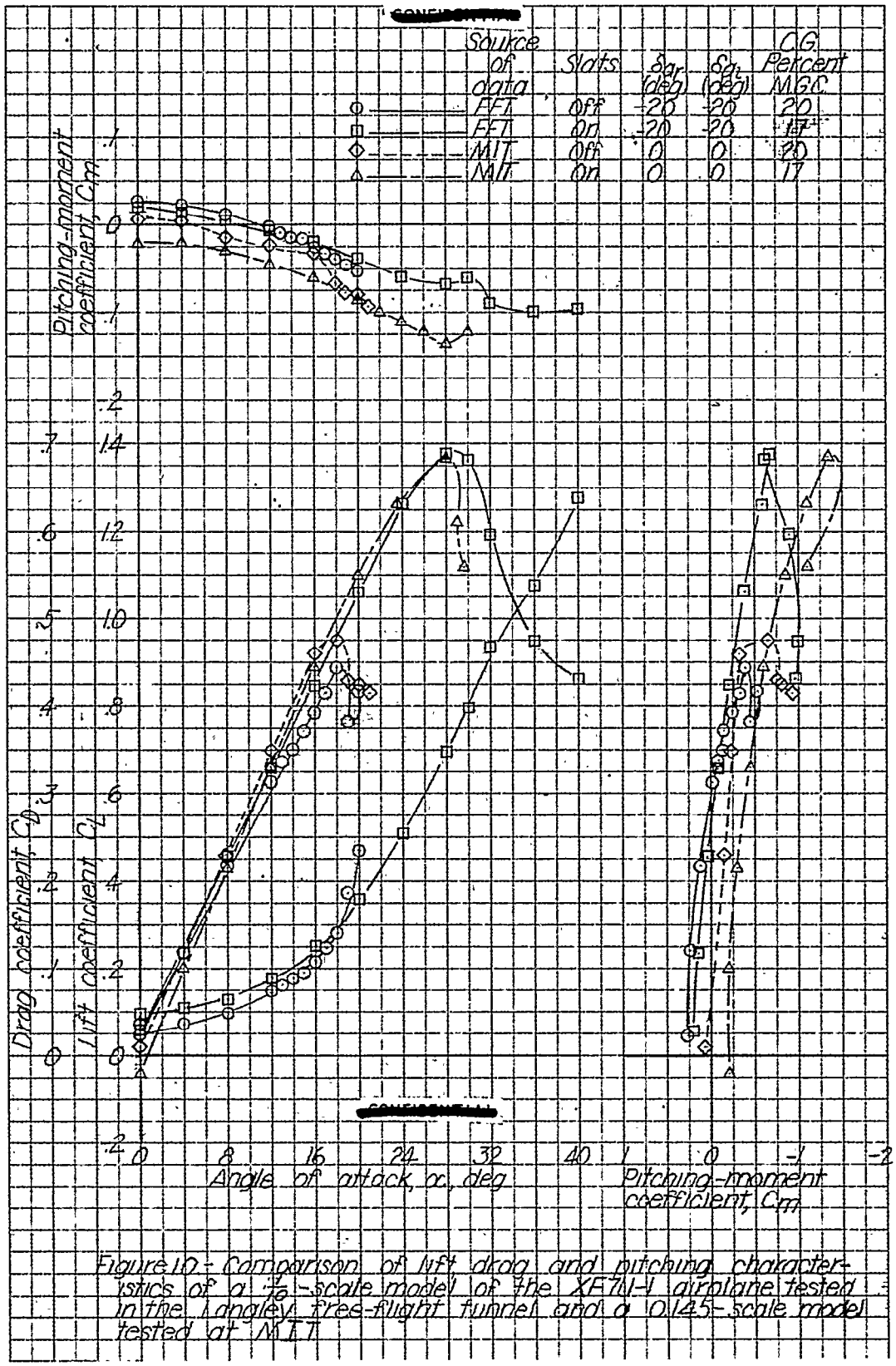

Figure 10 - Comparison of NFT drag and pitching characteristics of a $\frac{1}{10}$-scale model of the XF7U-1 airplane tested in the Langley free-flight tunnel and a 0.145-scale model tested at MIT.

NACA RM No. L8A19

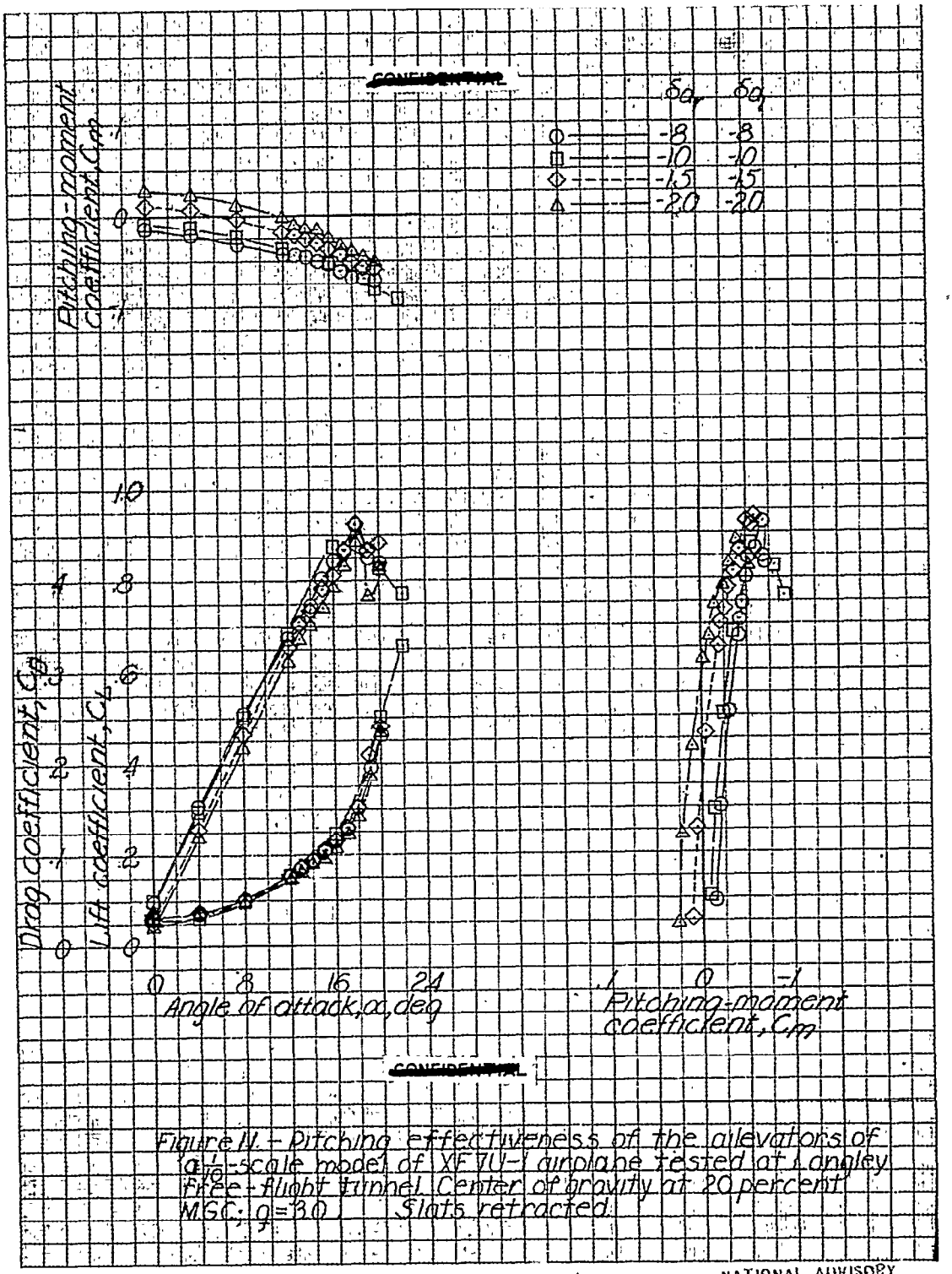

Figure IV.- Pitching effectiveness of the elevators of 1/6-scale model of XF7U-1 airplane tested at Langley free-flight tunnel. Center of gravity at 20 percent MGC; $i_t = 3.0°$; Slats retracted.

NATIONAL ADVISORY
COMMITTEE FOR AERONAUTICS

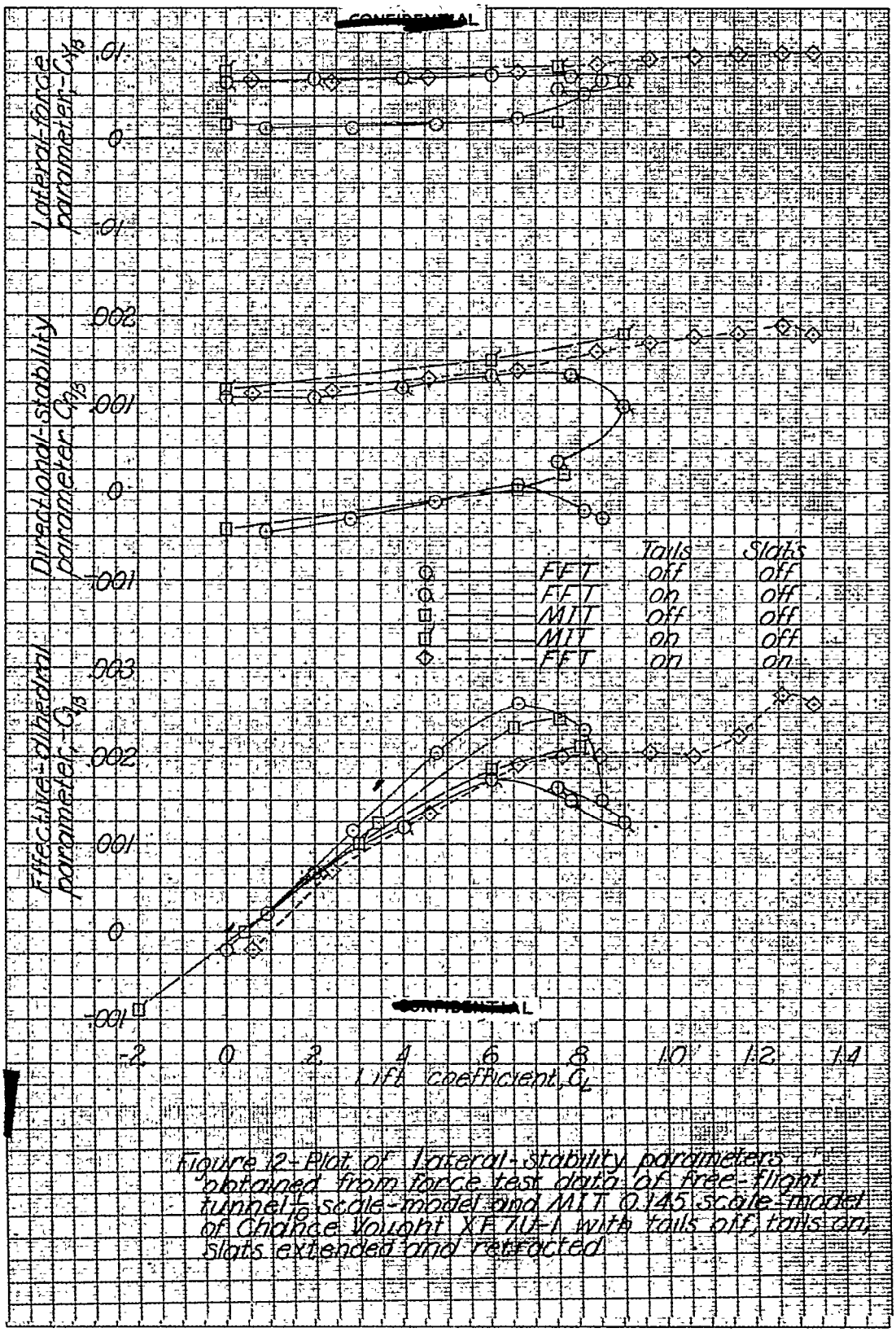

Figure 12.- Plot of lateral-stability parameters obtained from force test data of free-flight tunnel 1/6 scale-model and MIT 0.145 scale-model of Chance Vought XF7U-1 with tails off, tails on, slats extended and retracted.

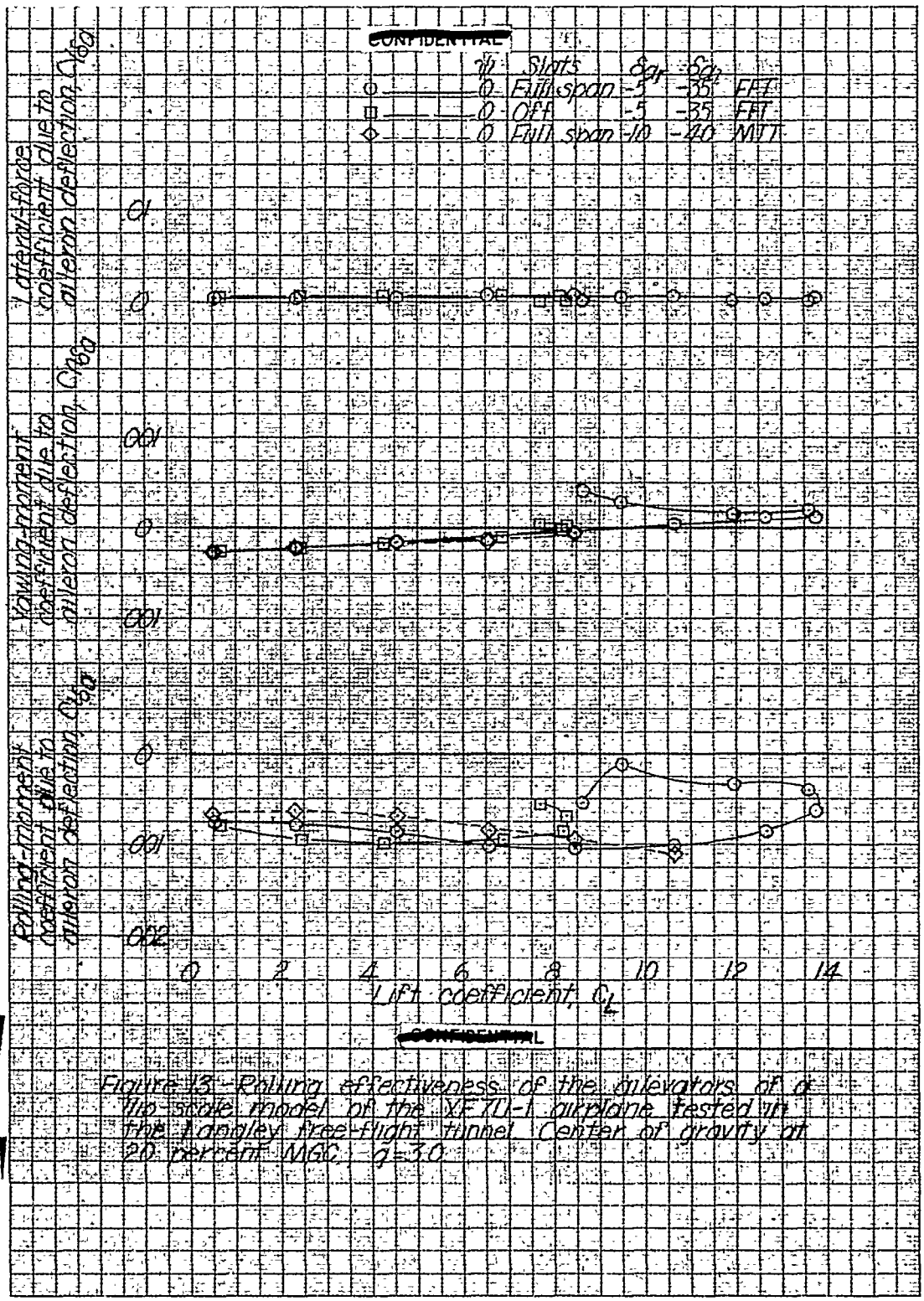

Figure 13.- Rolling effectiveness of the ailerons of a wing scale model of the XF7U-1 airplane tested in the Langley free-flight tunnel. Center of gravity at 20 percent MAC. $\eta = 3.0$

NATIONAL ADVISORY
COMMITTEE FOR AERONAUTICS

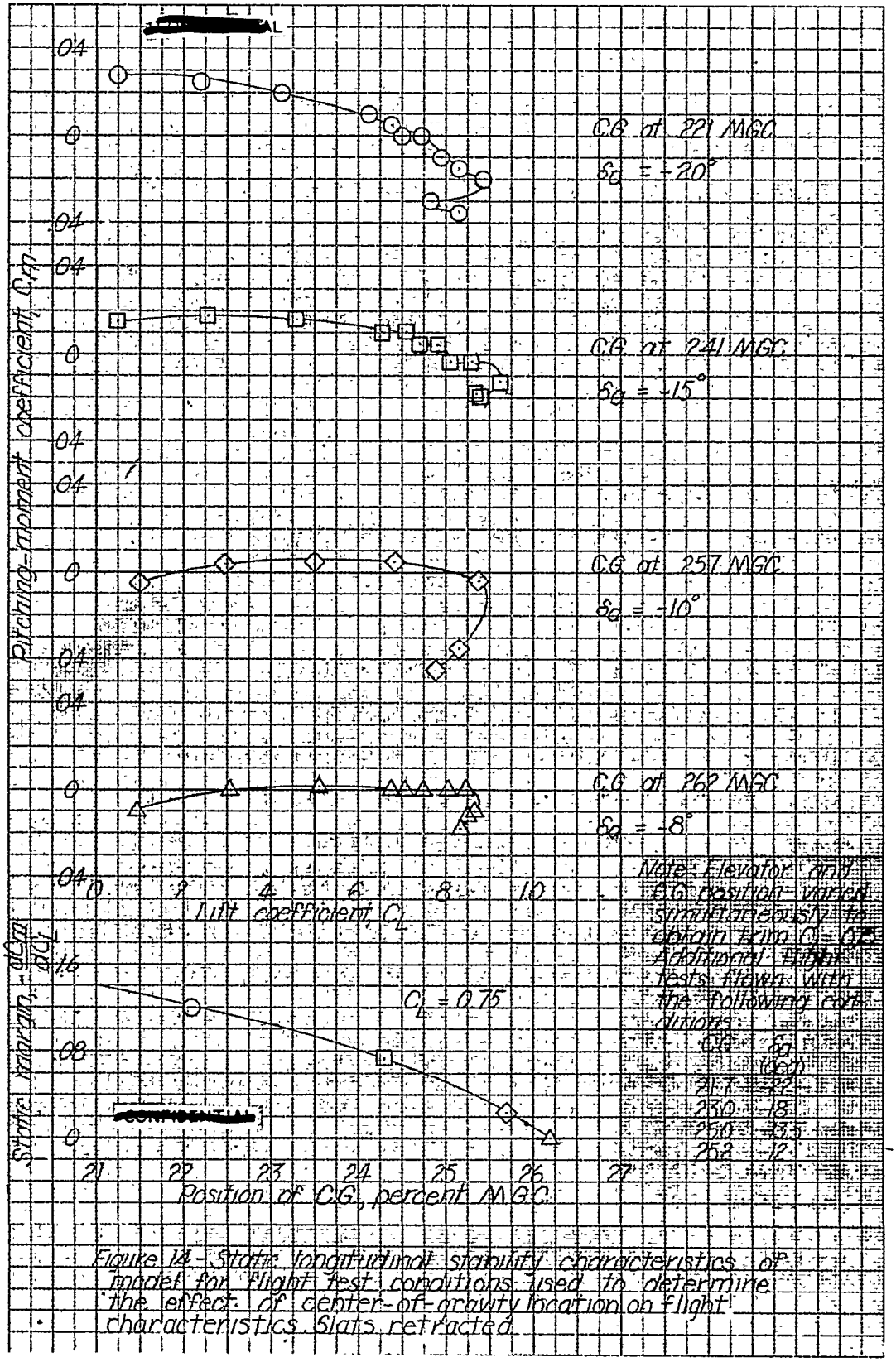

Figure 14.- Static longitudinal stability characteristics of model for flight test conditions used to determine the effect of center-of-gravity location on flight characteristics. Slats retracted.

NATIONAL ADVISORY
COMMITTEE FOR AERONAUTICS